Experimental and Modeling Study of Premixed Atmospheric-Pressure Dimethyl Ether−Air Flames

E. W. Kaiser,* T. J. Wallington,* and M. D. Hurley

Chemistry Department, Ford Motor Company, P.O. Box 2053, Mail Drop 3083/SRL, Dearborn, Michigan 48121-2053

J. Platz

The National Environmental Institute, Frederiksborgvej 399, DK-4000, Roskilde, Denmark

H. J. Curran,*,† W. J. Pitz,* and C. K. Westbrook

Lawrence Livermore National Laboratory, Livermore, California 94550

Received: November 16, 1999; In Final Form: June 29, 2000

Chemical species profiles have been measured at atmospheric pressure for two dimethyl ether (DME)−air flat flames having fuel/air equivalence ratios of 0.67 and 1.49. The samples, obtained with an uncooled quartz probe, were analyzed by either gas chromatography or Fourier transform infrared (FTIR) spectroscopy for CH_4, C_2H_2, C_2H_4, C_2H_6, C_3H_8, DME, CO, CO_2, O_2, CH_2O, and formic acid. A pneumatic probe calibrated at a reference position in the burned gas by a radiation-corrected thermocouple provided temperature profiles for each flame. Species profiles for two methane−air flames with equivalence ratios and cold-gas flow velocities similar to those of the DME flames were also obtained for comparison to the DME results. Mole fractions of C_2 product species were similar in DME and methane flames of similar equivalence ratios. However, the CH_2O mole fractions were 5−10 times larger in the DME flames. These experimental profiles are compared to profiles generated in a computer modeling study using the best available DME−air chemical kinetic mechanism. The Appendix presents photographs of DME, methane, and ethane diffusion flames. These results show that, while DME produces soot, its yellow flame luminosity is much smaller than that of an ethane flame at the same fuel volume flow rate, consistent with the low soot emission rate observed when DME is used as a diesel fuel.

Introduction

There is interest in improving motor vehicle fuel economy while complying with emissions regulations. Diesel engines offer improved fuel economy compared to gasoline vehicles, but NO_x and particulate matter will be difficult to control to proposed future emissions standards. With modern spark-ignition engines operating at stoichiometry, NO_x emissions are controlled by a three-way catalytic converter, and particle emissions are low. Because diesel engines operate fuel lean, control of NO_x by a catalyst becomes difficult. Diesel particulate emissions are higher than from spark ignition engines and can be reduced via traps, fuel additives, or changes in engine operating strategy. Reduction of feedgas emissions of these two regulated pollutants is confounded by the fact that engine operating conditions leading to reduced particulate matter result in higher NO_x emissions and vice versa.

Several recent publications have presented results from diesel engines or diesel vehicles operated on pure dimethyl ether (DME).[1−6] These experiments showed that DME is an excellent diesel fuel with a high cetane rating. This fuel produces very low particulate emissions, while the NO_x emissions are similar to those from current diesel fuel under the same engine operating conditions.[4] This allows the engine operating conditions to be adjusted to reduce NO_x without an accompanying increase in particulate emissions.[7]

Compression-ignition (diesel) engines require fuels that ignite easily. The ignition efficiency is defined by the cetane number of the fuel, which must be relatively high (>40−50) for a good diesel fuel. The high cetane rating that characterizes DME (>50) is in contrast to the very low cetane rating of branched ethers such as methyl *tert*-butyl ether (MTBE), which are difficult to ignite by compression and are used as octane enhancers in spark-ignition engine fuels. Because of the possible importance of DME as an alternative diesel fuel and because of the dramatic difference in ignition characteristics of ether fuels, there has been substantial interest in the oxidation chemistry of DME. This chemistry has been discussed in detail in recent publications for a variety of experimental conditions.[8−10] To explore the high-temperature oxidation chemistry of DME further, we have measured the chemical species profiles of two DME flames (one fuel-rich, one fuel-lean) stabilized on a flat-flame burner at atmospheric pressure. In addition, chemical species profiles have been obtained in rich and lean methane−air flames of similar fuel/air ratio for comparison to the DME experiments. These experimental profiles are compared to simulated profiles using the best available chemical kinetics mechanism. Finally, the luminosities of DME, CH_4, and C_2H_6 diffusion flames have been examined qualitatively to determine relative soot formation tendencies based on particulate blackbody emission.

* To whom correspondence should be addressed.

† Current address: Chemistry Department, Galway-Mayo Institute of Technology, Dublin Road, Galway, Ireland.

10.1021/jp994074c CCC: $19.00
Published on Web 08/17/2000

Experimental Measurements

Chemical species profiles were measured on a flat-flame burner supplied by McKenna Products, Inc. (Pittsburg, CA). This burner consists of a central, water-cooled, porous plug 6.02 cm in diameter, formed from bronze beads, through which the unburned fuel and air mixture passes. This central region is surrounded by a porous ring carrying a nitrogen gas flow to isolate the flame from the surrounding air. Samples were taken from the center of the burner through an uncooled quartz probe, which was mounted on a micrometer stage for vertical adjustment of the probe position relative to the burner surface. The probe was constructed from a 0.64-cm-diameter quartz tube drawn to a cone at the end. A hole, placed in the end of this cone, was determined to be approximately 0.003 cm in diameter, as estimated from the measured mass flow rate through the orifice using the standard equation for choked flow. The probe tip intersected the plane of the flame at an angle of approximately 80°.

Samples were withdrawn from the flame through the probe into a vacuum manifold and stored in Pyrex sample flasks at reduced pressure. The maximum pressure of the samples was restricted to 10 Torr to minimize reactions occurring within the hot tip of the probe after sampling.[11] These samples were analyzed either by gas chromatography (GC) or by Fourier transform infrared (FTIR) spectroscopy. Species quantified by GC were CH_4, C_2H_2, C_2H_4, C_2H_6, C_3H_8, DME, CO, CO_2, and O_2. Those measured by FTIR were CH_4, C_2H_2, C_2H_4, DME, CO, CO_2, CH_2O, and HOCHO (formic acid). In addition to the 10-Torr samples, the maximum sample pressures for selected experiments on the DME flame were allowed to rise to 30 Torr to examine the effect of sample pressure on the measured species concentrations. Increasing the final sample pressure increases the average residence time of the gas in the hot zone of the probe after sampling as the mass flow rate through the choked orifice remains constant. As discussed elsewhere,[11] if the effect of sample pressure on the measured species concentrations in the sample is small, perturbation of the samples by continuing oxidation in the hot portion of the probe must also be small.

It is possible that, during the sampling process, some of the low-concentration organic species might adsorb on the walls of the cool regions of the probe, the transfer tubing, the vacuum manifold, or on the walls of the storage flask. To investigate this possible perturbation, known concentrations of CH_4, CH_2O, or formic acid were prepared in air diluent within a Pyrex flask. The tip of the sample probe was inserted into this flask, and a sample was withdrawn through the same vacuum manifold described above into the sample flask used in the experiments. The three species chosen cover a wide range of absorptivity from methane, which is not expected to adsorb at all, to formic acid, which is a polar molecule and could potentially adsorb significantly on surfaces. FTIR analyses of these test samples showed that no loss of any of these species occurred during sampling to within the estimated 10% experimental error. These experiments verify that sampling losses for the species measured will be less than the experimental data scatter and need not be considered further.

Chemical species profiles and temperature profiles were measured for four atmospheric-pressure fuel−air flames during these experiments, two each for DME and CH_4 fuels. The DME flames had fuel/air equivalence ratios ($\phi = [F/A]/[F/A]_{stoic}$) of 0.67 (fuel-lean) and 1.49 (fuel-rich). These ratios were determined from a combination of the measured fuel and air flow rates and the chemical composition of the burned gas (CO and CO_2). They are estimated to be accurate to ±3%. The linear cold-gas flow velocity at 298 K (8.66 and 8.57 cm/s for the lean and rich DME flames, respectively) was determined from the measured reactant gas flow rates and the known burner diameter assuming a uniform flow across the surface of the burner. The methane flames had fuel/air equivalence ratios (±3%) of 0.74 and 1.47 with cold-gas flow velocities of 8.66 and 9.32 cm/s for the lean and rich flames, respectively.

Measurements of species profiles in burner flames are often carried out at reduced pressure, broadening the flame front to several millimeters and making accurate probe position measurements easier. However, for testing chemical kinetic mechanisms under conditions more typical of practical combustors, studies of atmospheric-pressure flames are very important and are the subject of this paper. These flames have thicknesses in the range of 1−2 mm, and variations in species concentrations of factors of 10 over a few tenths of a millimeter are typical. From the reproducibility of our species profiles upon extinguishing and relighting the flames, the absolute accuracy of the probe positioning relative to the flame position is estimated to be ±0.15 mm. Thus, in comparisons of experimental species concentrations to modeling calculations, deviations of 0.1−0.2 mm in absolute position are not deemed significant. However, the shapes of the species profiles are more reproducible and deviate by <0.1 mm. In addition, the peak concentrations of intermediate and final combustion products are reproducible to better than 15% upon remeasurement after extinguishing and relighting of the flame. They are also independent of the analytical technique (GC or FTIR). These results indicate that the data are sufficiently reproducible to be useful for model validation at atmospheric pressure.

Temperature Profiles. The temperature of the burned gas was measured in each flame by a Pt−Pt(13% Rh) thermocouple with a 0.015-cm-diameter bead, corrected for radiation losses using a technique described elsewhere.[12] The thermocouple wires were sheathed in a ceramic tube for support. Both the bead and the exposed wire leads (1-cm-long) beyond the support tube entered the flame vertically. Because the leads descended vertically into the flame, this thermocouple could not be used to measure temperatures in the preheat zone below the flame because conduction of heat through the leads, which remained in the hot burned gas, caused the bead to be substantially hotter than the actual gas temperature. However, because the temperature profile in the burned gas decreases very slowly with increasing height, the leads and bead will be at nearly the same temperature when they are both in the burned gas, and the effects of conduction through the leads will be small. On the basis of previous data, this thermocouple produces temperature measurements with better than ±40 K accuracy in the burned gas relative to a spectroscopic temperature determination.[12]

To measure the temperature through the flame zone, the sampling probe was used as a pneumatic temperature-measuring device by determining the rate of flow of gases into a known volume as a function of the probe position in the flame. In principle, the absolute temperature could be determined from these data using the equation for choked flow,[13] but this requires exact knowledge of the throat area, which is not easy to obtain. Therefore, we have chosen to calibrate the pneumatic temperature measurement using the temperature of the burned gas as determined by thermocouple at a chosen reference position. The equation for choked flow is then applied to obtain the relative temperature profile throughout the flame zone. From the choked flow equations, the temperature at any given point in the flame relative to that at the reference position (T_{ref}) in the burned gas is obtained from the equation

$$(T_1/T_{ref}) = (f_{ref}/f_1)^2(M_{ref}/M_1)$$

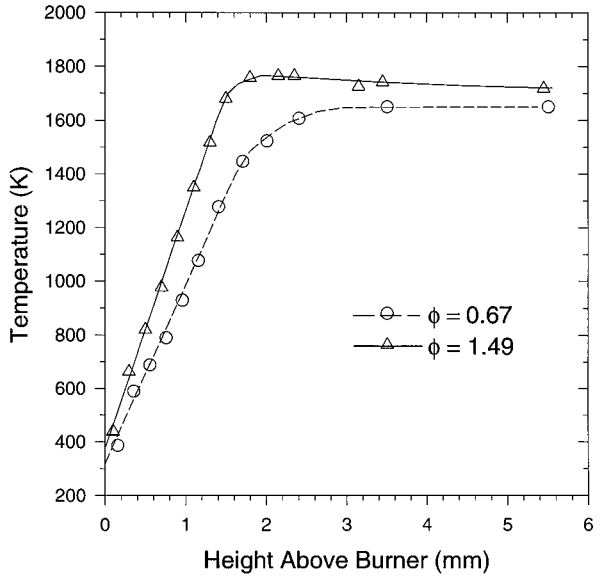

Figure 1. Temperature profiles of the fuel-lean ($\phi = 0.67$) and fuel-rich ($\phi = 1.49$) atmospheric-pressure DME−air flames plotted as a function of position relative to the burner surface. Top of the luminous flame zone: lean flame (2.13 mm); rich flame (1.35 mm). Individual points = experimental data; lines = temperature profile used in the computer simulation.

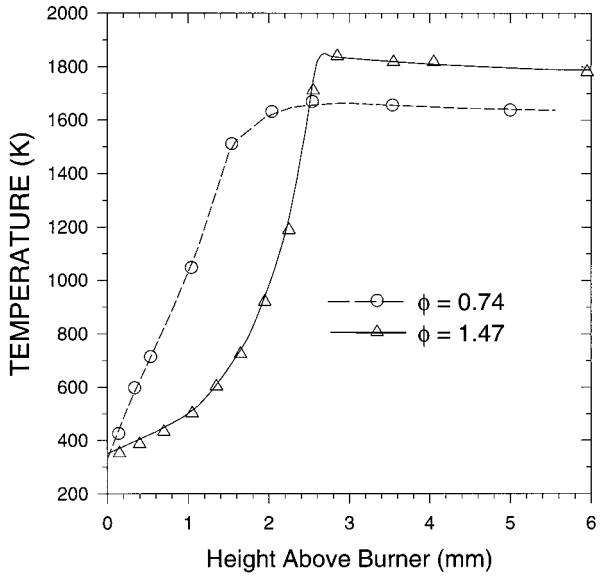

Figure 2. Temperature profiles of the fuel-lean ($\phi = 0.74$) and fuel-rich ($\phi = 1.47$) atmospheric-pressure methane−air flames plotted as a function of position relative to the burner surface. Top of the luminous flame zone: lean flame (1.5 mm); rich flame (2.3 mm). Individual points = experimental data; lines = temperature profile used in the computer simulation.

in which f_1 and f_{ref} represent the flow through the orifice (moles per second) at probe position 1 and at the reference position, respectively. M_1 and M_{ref} are the average molecular weights of the gases at position 1 and at the reference position, respectively. Applying this equation to the measured flow rate through the orifice as a function of probe position allows a calculation of the temperature through the flame and to the burner surface based on the value of T_{ref} measured in the burned gas by the thermocouple.

It might be argued that the probe can perturb the flame position during this measurement, thereby leading to an incorrect temperature profile. Although this is certainly possible, there is no visible perturbation of the flame front as the probe is lowered. In addition, as stated by Fristrom:[14] "The advantage of using the pneumatic probe is that it allows a probe simultaneously to measure temperature and composition. This avoids difficulties in alignment of profiles." Although we did not actually measure temperature and composition in the *same* experiment (two experiments were used, one for species and one for temperature), probe perturbation of the flame will be similar when the probe is used to measure either species or temperature. Thus, this technique should provide the most consistent species and temperature profiles possible in a probe-based experiment.

Figures 1 and 2 present the temperature profiles measured for the DME and methane flames, respectively. For all of the flames, the temperature rises sharply in the preflame zone and reaches a peak slightly above (0.2−0.3 mm) the top of the luminous flame zone after the CO conversion to CO_2 is complete. For all four flames, the temperature profile extrapolates to near ambient at the burner surface, providing evidence that the pneumatic probe technique used to measure the temperature profile yields results of reasonable accuracy.

Assuming a cold gas temperature of 300 K, the calculated adiabatic flame temperatures (T_{ad}) for DME are 1873 K (lean) and 2057 K (rich). For the methane flames, T_{ad} is 1900 K (lean) and 1924 K (rich). The peak flame temperatures measured in these experiments are 200−300 K below T_{ad} for all flames except the rich methane−air flame. The peak temperature of this flame (1845 K) is only 80 K below adiabatic, and in fact, this flame is observed to be nearing blow off. This is the reason the rich methane flame lies farther from the burner and has a temperature profile with a slower initial temperature rise than is observed for the other flames.

As an additional cross check of the measured maximum flame temperature for the lean DME flame, the flow rate of the water through the cooling coils in the burner and the increase in the water temperature during passage through the burner were measured. At a water flow rate of 29.6 $cm^3\ min^{-1}$, the water temperature increased by 21 K, indicating that 622 cal min^{-1} was being withdrawn from the flame gases to the cooling water at the burner surface. From the estimated heat capacities of DME (0.34 cal $g^{-1}\ K^{-1}$) and air (0.24 cal $g^{-1}\ K^{-1}$) and the measured cold-gas flow rates (DME = 1.23 g min^{-1} and air = 16.67 g min^{-1}), the heat extracted to the water will lower the flame temperature by 140 K below T_{ad}. Therefore, the actual flame temperature is $T_f < T_{ad} - \Delta T_{water} = 1873 - 140 = 1733$ K. Note that this is an upper limit to the flame temperature because heat will also be lost from the burner to the surrounding supports and air. The above temperature is to be compared to the measured maximum temperature for the lean DME flame of 1650 ± 40 K, measured by thermocouple. The measured temperature is certainly consistent with and not too far below the upper limit calculated from the heat loss to the cooling water, lending additional support to the peak thermocouple temperatures.

Species Profiles. Prior to a discussion of the experimental species profiles, it is important to examine the effect of sampling pressure within the probe on the measured species concentrations. As mentioned earlier in the Experimental Measurements section, this provides an estimate of the effect of continuing oxidation of organics in the hot section of the probe during the sampling process, which can perturb the measured concentrations.[11] Therefore, the effect of sample pressure on species concentrations was examined for both DME flames. In the lean flame, the pressure dependence was examined in the preflame zone at heights of 1.08 and 1.66 mm above the burner. At both probe locations, the species concentrations (CO, CO_2, CH_2O, CH_4, C_2H_6, C_2H_4, C_3H_8, and DME) were unaffected by maxi-

mum sample pressure over the range 10−30 Torr to within the estimated 10−20% experimental uncertainty. This verifies that reactions within the sample probe do not affect the measured species concentrations in the lean flame for a maximum sampling pressure of 10 Torr. In the rich flame, variation of the sample composition with total sample pressure was measured at 0.75 and 1.35 mm above the burner surface. At the top of the luminous zone (1.35 mm), no change in sample composition (±15%) was observed as the sample pressure was varied. In the preflame zone at 0.75 mm, there were small but possibly significant decreases in the C_2H_6 (24%) and CH_2O (28%) concentrations as the pressure was reduced from 30 to 10 Torr. This indicates that, as the residence time in the probe increases, these two species may be formed to a small extent by reactions within the probe at this height. However, extrapolation of these curves to zero pressure to estimate the unperturbed species mole fractions[11] indicates that any correction to the data taken at 10 Torr will be less than 10%, which is on the order of the data uncertainty. Thus, all available evidence suggests that reactions inside the probe do not affect any of the measured species concentrations to a significant extent (<10%), provided that the sample pressure is limited to 10 Torr, as has been observed previously.[11]

Each of the atmospheric-pressure flat flames has a thin (e.g., 0.5−1.5 mm) luminous zone that is deep blue for lean flames and blue-green for rich flames. The thickness of the luminous zone can be estimated with good reproducibility (±0.1 mm based on repeat measurements) using the sampling probe as a measuring device with the room lights dimmed to provide good visibility. The probe is slowly lowered from the burned gas region until the tip is observed to touch the top of the luminous zone when viewed edge-on through a magnifying lens. The probe is then lowered until the tip reaches the bottom of the luminous zone. The difference in the two probe heights provides an estimate of the luminous zone thickness. Although it is possible for the probe to slightly perturb the flame, this will not affect the thickness measurement appreciably because the luminous zone is viewed from its edge. Thus, this zone is observed across the entire width of the burner, while any flame perturbation occurs only in a small region around the probe tip. These measurements are presented as the "luminous zone" in Figures 3−6. For all flames except that of lean DME, the luminous zones are relatively narrow (0.4−0.6 mm). In contrast, the lean DME flame has a significantly broader luminous zone (1.5 mm) that extends to within 0.6 mm of the burner surface. The luminous zone of this flame is broader than that of the three other flames in this study and broader than observed previously for a lean propane−air flame.[11] The luminous zones of the lean and rich DME flames were also photographed edge-on using a digital camera with an aperture of $f = 3.4$ and a shutter speed of 1/60 s to verify the probe-based measurement. A typical photograph for each flame is shown in the Appendix. The scale for these photographs can be estimated by observing the diameter of the flame disk for the brighter rich flame, which is approximately equal to the diameter of the burner (6.0 cm). The vertical axis of each digital photograph has been expanded by a factor of 4 for improved clarity. It is evident that the lean flame is much thicker than the rich flame. The thickness of the lean flame is 1.5 mm based on the photograph, identical to that estimated by the probe measurement described above (Figure 3). The rich flame has a very bright zone 0.4 mm thick and a much dimmer region extending another 0.25 mm. The thickness of the bright region of this flame is identical to that measured by the probe technique (Figure 4).

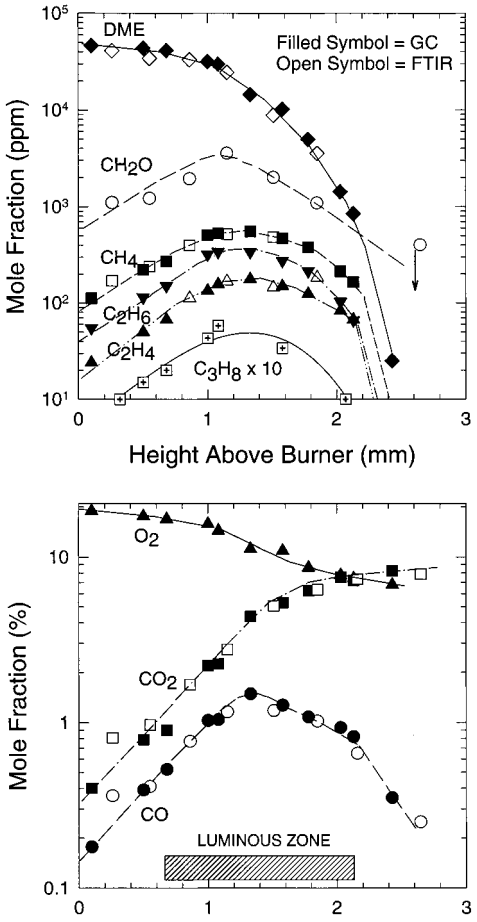

Figure 3. Species profiles for the fuel-lean ($\phi = 0.67$) DME−air flame plotted as a function of sample probe position. Mole fractions were obtained by either GC (filled symbols) or FTIR (open symbols) analyses. The location of the luminous flame zone is indicated as a crosshatched box. The symbols for organic species in Figures 3−6 represent: DME, diamond; CH_2O, circle; CH_4, square; C_2H_4, triangle; C_2H_6, inverted triangle; C_2H_2, hexagon; and C_3H_8, square with +. Formic acid < 100 ppm. At 2.4 mm, $CH_4 = 2$ ppm; $C_2H_4 = C_2H_6 = 0.3$ ppm. Downward arrow (CH_2O) = upper limit. Maximum $C_2H_2 \approx 10$ ppm at 1.2 mm.

Figures 3 and 4 present the measured species profiles in the lean and rich DME−air flames, respectively. Also shown in the figures is the position and thickness of the [blue (lean) and blue-green (rich)] luminous zone for each of these flames relative to the burner surface, measured as described above. Figures 5 and 6 present comparable species profiles for the lean and rich methane−air flames, respectively. The data points for the lean DME flame were obtained from three GC and two FTIR profile measurements in which the flame was extinguished and relighted for each data set to determine reproducibility. For the rich DME flame (Figure 4), four GC and three FTIR data sets were obtained. The data scatter indicate that the measured species mole fractions are reproducible to ±10% for both DME flames, and the probe position is consistent to ±0.07 mm.

The lean methane-flame data in Figure 5 were obtained from one GC and two FTIR experiments, each of which represent a resetting of gas flows and reignition of the flame. These data are also reproducible to ±10% in mole fraction and 0.07 mm in probe position. For the rich methane−air flame, the FTIR data were obtained from three separate measurements and are reproducible. However, the raw species profiles for the single GC measurement were shifted approximately 0.25 mm closer to the burner surface, although the species profile shapes were indistinguishable from the FTIR data. Because this flame is near

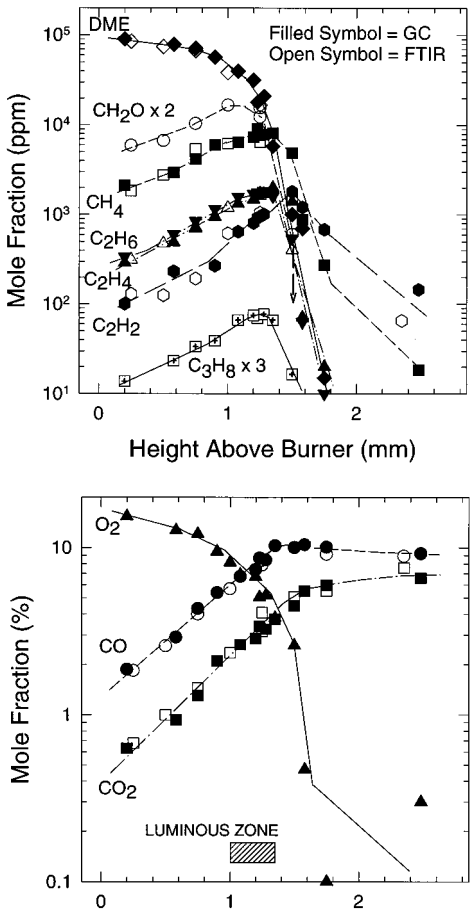

Figure 4. Species profiles for the fuel-rich ($\phi = 1.49$) DME−air flame plotted as a function of sample probe position. Mole fractions were obtained by either GC (filled symbols) or FTIR (open symbols) analyses. Location of the luminous flame zone is indicated as a crosshatched box. Downward arrow at 1.5 mm (CH_2O) = upper limit. For symbol identification, see Figure 3.

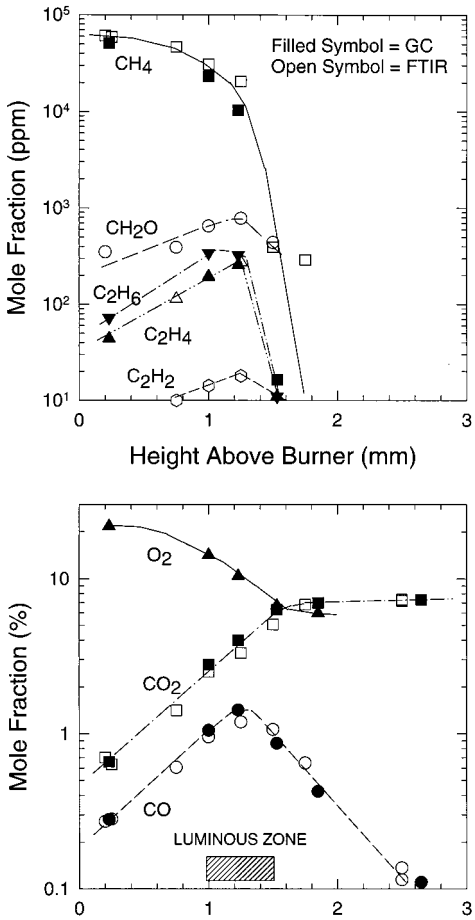

Figure 5. Species profiles for the fuel-lean ($\phi = 0.74$) methane−air flame plotted as a function of sample probe position. Mole fractions were obtained by either GC (filled symbols) or FTIR (open symbols) analyses. Location of the luminous flame zone is indicated as a crosshatched box. For symbol identification, see Figure 3.

blow off, slight inaccuracies in the gas flows may cause significant changes in the location of the flame upon resetting of the gas flows. For this flame only, the measured probe positions for the GC data have been adjusted by +0.25 mm such that the CH_4 profile overlaps that of the FTIR data. For the other three flames, no adjustment was made to any of the experimental probe positions. In the rich methane flame, we estimate the reproducibility to be ±0.2 mm in the absolute location of the probe relative to the flame zone upon resetting the gas flows.

In both DME flames, the major organic species is CH_2O, but appreciable mole fractions of the hydrocarbons CH_4, C_2H_4, and C_2H_6 are also present. C_2H_2 is an important species only in the rich flame, as observed in studies of propane−air flames[11] and in other flame studies. CH_4 is the highest-concentration hydrocarbon species produced in both DME flames, equaling the concentration of CH_2O in the rich DME−air flame. The observation of appreciable quantities of C_1 and C_2 hydrocarbon species demonstrates the presence of a substantial concentration of methyl radicals in these DME flames. Because formic acid has been observed in other DME oxidation experiments, the FTIR spectra were searched for the sharp and relatively strong absorption line characteristic of formic acid. No formic acid was observed to within the estimated detectability in our system (approximately 100 ppm) in either DME flame. C_3H_8 was observed and quantified in the flame zones of both DME flames. C_3H_6 could not be measured because a very small quantity of C_3H_6 (20 ppm) was present in the unburned gas flow stream as an impurity in the DME. Thus, we estimate that the amount of C_3H_6 formed is <25 ppm in both flames. No other C_3 species was observed at concentrations >5 ppm.

In comparisons of the rich and lean DME flame profiles to the corresponding profiles for the methane flames, it is apparent that the peak concentrations of the C_2 species are similar for both fuels. However, the CH_2O mole fraction is much higher in the DME flames. This is particularly apparent in the rich flame for which the CH_2O mole fraction is ∼10 times larger than that in the rich methane−air flame. The minimum detectable CH_2O mole fraction in the FTIR measurements is ∼250 ppm, and the measured CH_2O mole fractions have spectral uncertainties of ∼10%. These observations indicate that the DME flames have a much larger source channel for CH_2O formation than do the methane flames. However, the concentration of methyl radicals must be comparable in flames from both fuels as the C_2 species have similar peak mole fractions and are likely to be formed from bimolecular reactions of methyl radicals. These results suggest that dissociation of methoxymethyl radicals

$$CH_3OCH_2 = CH_3 + CH_2O$$

which are formed by the initial free radical attack on DME in the flame, is a very important channel in the high-temperature flame chemistry of DME, because this channel is a major source of methyl radicals in the chemical mechanism. It also provides a major source of CH_2O via a channel that is not present in the methane oxidation mechanism. Therefore, this reaction channel

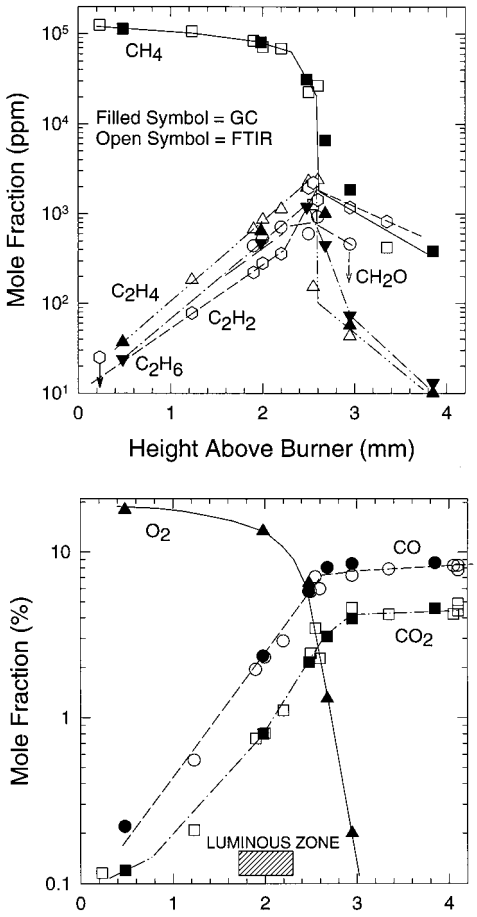

Figure 6. Species profiles for the fuel-rich ($\phi = 1.47$) methane−air flame plotted as a function of sample probe position. Mole fractions were obtained by either GC (filled symbols) or FTIR (open symbols) analyses. Location of the luminous flame zone is indicated as a crosshatched box. Downward arrows (CH_2O, C_2H_2) = upper limit. For symbol identification, see Figure 3.

can provide a rationale for the observation that the C_2 intermediate oxidation product mole fractions are similar for the two fuels but that DME flames produce much higher mole fractions of CH_2O. In the CH_4 flames, C_3H_8 was observed but not quantified. Peak mole fractions did not exceed 20 ppm at either equivalence ratio.

The O_2 mole fraction measured near the burner surface in the lean methane−air flame exceeds that in pure air diluted by the initial CH_4 by 20%. This indicates that, for this flame only, the O_2 determination was incorrectly calibrated, and the true O_2 mole fraction should be 20% lower throughout the flame. Because O_2 data are not critical to the comparison with the simulated profiles, the data were not retaken. However, in the simulation portion, the experimental O_2 in this flame has been reduced by 20%.

Another measure of the reproducibility of the species measurements can be obtained by comparing the data for the lean methane flame in Figure 5 to those obtained from a similar, but not identical, flame condition in earlier experiments.[15] In these earlier experiments, the equivalence ratio was identical to that in Figure 5, but the cold-gas flow velocity was slightly lower (7.6 vs 8.66 cm/s). The peak concentrations of CO, C_2H_6, and C_2H_4 in the earlier experiments (1.2%, 330 ppm, and 240 ppm, respectively) are identical to those in Figure 5 (1.4%, 350 ppm, and 280 ppm) to within the ±10% data scatter. (Previous experiments with fuel-rich propane−air flames have shown that the peak species concentrations are not influenced strongly by changes of 50% in cold-gas flow velocity.[11]) In addition, the location of the tops of the luminous zones are essentially identical [1.6 (ref 15) vs 1.5 mm above the burner]. The fact that the current probe orifice diameter is 30 μm vs 120 μm in ref 15 is the reason that the mole fractions in Figure 5 decrease more rapidly as the probe approaches the burner than in the earlier experiments. A large diameter orifice perturbs the species concentrations more than a small diameter orifice near the burner surface.[15]

Computational Model

The detailed chemical kinetic reaction mechanism used in these calculations is based on a previously published reaction mechanism[8] and on an updated mechanism.[9,10] The full mechanism used in this work is documented in ref 10. All reaction numbers given in this paper refer to the numbering sequence there. The transport parameters for the species were obtained from the CHEMKIN database,[16] Marinov et al.,[17] and Reid, Prausnitz and Poling.[18] When data were not available, the transport parameters of the radicals were estimated from those of the parent species. The experimental temperature profiles versus distance above the burner (Figures 1 and 2) were used as input in the simulation of these flames. Modeling simulations were carried out using CHEMKIN III[19] with the PREMIX package[20] and with the HCT modeling code.[21] The chemical kinetic mechanism, developed using the HCT code, was converted in order to make it compatible with the CHEMKIN format. In doing so, both forward and reverse rate constant expressions were included in the CHEMKIN chemistry linking file to avoid any potential differences that thermodynamic properties might have on equilibrium constants and overall rates of reaction. The PREMIX code was employed for the final fits to the data because it is used extensively by the combustion community in modeling burner-stabilized flames. Overall, the results obtained using the HCT and CHEMKIN III codes are very similar but not identical (Figure 7a and b). We were unable to identify the reasons for the differences in the HCT and PREMIX predictions. These differences could result from differences in the gridding of the domain of the one-dimensional flame. In HCT, each grid line is specified manually, whereas in PREMIX, grid lines are added to regions of high gradient or curvature. However, we did double the number of grid lines in HCT without significant improvement in the comparison between HCT and PREMIX.

Comparisons of the experimentally measured (symbols) and PREMIX-predicted (lines) species profiles versus distance above the burner for the DME flames are provided in Figures 8 and 9 and for the methane flames in Figures 10 and 11. Overall, there is good agreement between model and experiment, with the relative concentration of intermediate species correctly reproduced by the model, and in most cases, the absolute values are in good agreement. Some modeling deficiencies are addressed in the discussion below.

The physical and chemical processes controlling the fate of reactants, products, and important intermediate species throughout the flame were analyzed using both the PREMIX and HCT computer codes. The PREMIX postprocessor code provides details about which chemical reactions are important in producing and consuming species of interest. Information on the effect of diffusion and convection on species concentrations throughout the flame was provided by the HCT code because it was not available from the PREMIX postprocessor. In reviewing these edits, we are able to gain a detailed description of the factors influencing fuel oxidation and intermediate formation and consumption across the flame. It is particularly interesting to

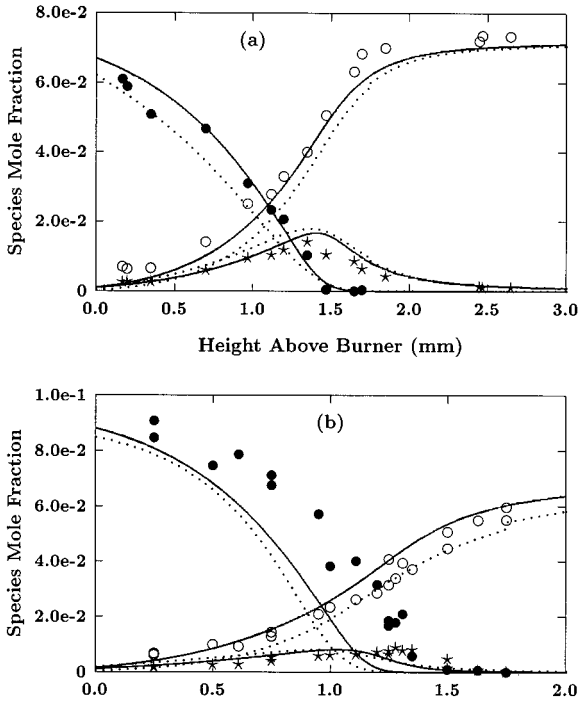

Figure 7. (a) Comparison of CHEMKIN (solid lines) and HCT (dotted lines) for the fuel-lean ($\phi = 0.74$) methane−air flame plotted as a function of sample probe position. ●, CH_4; ○, CO_2; and ★, CO. (b) Comparison of CHEMKIN (solid lines) and HCT (dotted lines) for the fuel-rich ($\phi = 1.49$) DME−air flame plotted as a function of sample probe position. ●, CH_3OCH_3; ○, CO_2; and ★, CO.

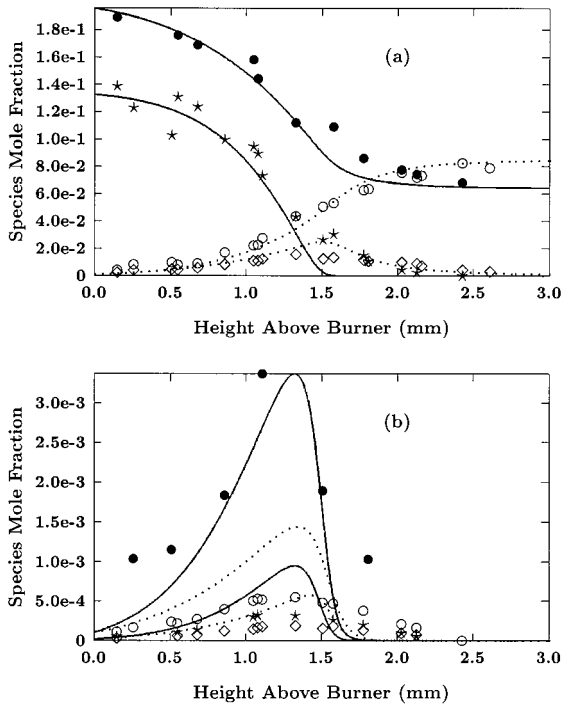

Figure 8. (a) Species mole fractions for the fuel-lean ($\phi = 0.67$) DME−air flame plotted as a function of sample probe position. ●, O_2; ○, CO_2; ★, CH_3OCH_3 (×3); and ◇, CO. (b) Symbols for experimental data and computed peak concentrations for intermediate species (to aid curve identification) are ●, CH_2O (3370 ppm); ○, CH_4 (1435 ppm); ★, C_2H_6 (950 ppm); and ◇, C_2H_4 (590 ppm). Solid lines correspond to calculated mole fractions for filled and dotted lines to open symbols.

examine the physical and chemical factors controlling the species in this flame, as a DME flame has not been analyzed numerically before.

Lean Dimethyl Ether Flame. Figure 8 depicts species concentration profiles versus height above the burner surface for the lean ($\phi = 0.67$) dimethyl ether flame. The main species measured experimentally were the fuel and molecular oxygen together with the main oxidation products CO, CO_2, CH_2O, CH_4, C_2H_6, and C_2H_4. The simulated fuel profile is in good agreement with the experiment up to about 1.1 mm above the burner surface. However, at positions higher than this the simulation predicts a much faster rate of fuel consumption than that measured in the experiments, which show a more gradual rate of fuel oxidation (Figure 8a). The simulated O_2 profile shows the same behavior but to a lesser degree. Because of the rapid fuel consumption, the peak heights for all of the intermediate species except CH_2O are overpredicted relative to the experimental measurements, the greatest disagreement being in the overprediction of methane concentrations and the related ethane and ethylene profiles by about a factor of 3. In addition, the experimental species profiles are broader than those predicted by the model. This disagreement between model and experiment must be due to some deficiency in the kinetic mechanism, perhaps in the exclusion of a chemically activated pathway of the methoxymethylperoxy radical producing two molecules of formaldehyde and a hydroxyl radical.[22]

$$CH_3OCH_2 + O_2 = CH_3OCH_2O_2^* = CH_2O + CH_2O + OH$$

Analysis of the HCT edits indicates that diffusion and convection downstream are main factors controlling fuel and oxygen profiles up to a distance of 0.8 mm, where the temperature is 850 K. In this zone (at this position), the concentration of DME is approximately 75% of that flowing in through the burner surface. The concentration of DME is mainly controlled by diffusional transport of DME and by the consumption of DME by chemical reaction. The ratio of net loss of DME by diffusional transport to net loss by chemical reaction is 5.5:1. The main reactions controlling fuel chemistry are H-atom abstractions from the fuel by OH radicals, by H atoms, and by CH_3 radicals in the ratio 5:3:1. The methoxy radical, formed primarily by the reaction of methyl and hydroperoxyl radicals, decomposes in this zone to produce formaldehyde and hydrogen atoms, which also diffuse into this zone, having been generated downstream. Hydroxyl radicals are also formed primarily by the reaction of methyl radicals with hydroperoxyl radicals, as depicted below. Methyl radicals are mainly formed from the decomposition of the methoxymethyl radical, which also generates formaldehyde ($CH_3OCH_2 = CH_2O + CH_3$).

At 1.3 mm above the burner surface (1185 K), the concentration of the fuel is approximately 28% of that entering the flame. Approximately 80% of fuel consumption occurs via hydrogen abstraction from the fuel, with diffusion and convection each responsible for carrying about 10% of the fuel downstream. Of the chemistry, hydrogen-atom abstractions by hydroxyl radicals and hydrogen atoms are the most important with abstraction by OH being about 40% greater than that by H. Hydroxyl radicals are generated via the following reactions:

$$CH_3 + HO_2 = CH_3O + OH \quad (22)$$

$$HO_2 + H = OH + OH \quad (47)$$

$$H + O_2 = O + OH \quad (8)$$

$$CH_3OCH_3 + O = CH_3OCH_2 + OH \quad (267)$$

(The reaction numbers refer to ref 10, where the mechanism is

documented.) Hydrogen atoms mainly diffuse into this zone from a position downstream and are consumed by reactions with the fuel, formaldehyde, and molecular oxygen.

$$CH_3OCH_3 + H = CH_3OCH_2 + H_2 \quad (275)$$

$$CH_2O + H = HCO + H_2 \quad (33)$$

$$H + O_2 = O + OH \quad (8)$$

At this location, the concentration of molecular oxygen is 64% of that entering the flame. Approximately 62% of oxygen consumption occurs via diffusion and 7% via convection downstream, away from the burner surface, whereas 31% is consumed by chemical reaction, mainly with formyl radicals and hydrogen atoms.

At 1.3 mm above the burner surface, the concentrations of formaldehyde, methane, and ethane each reach their peak. Formaldehyde is mainly produced by the β-scission of the methoxymethyl radical (66%) and the methoxy radical (33%). Methane is generated through abstraction of hydrogen atoms by methyl radicals from stable species (mainly DME), whereas ethane is formed from the recombination of methyl radicals (R24, where "R24" indicates reaction 24). Ethylene is generated from the decomposition of ethyl radicals.

$$CH_3OCH_2 = CH_2O + CH_3 \quad (282)$$

$$CH_3O = CH_2O + H \quad (40)$$

$$CH_3 + HO_2 = CH_4 + O_2 \quad (45)$$

$$CH_3OCH_3 + CH_3 = CH_3OCH_2 + CH_4 \quad (279)$$

$$CH_2O + CH_3 = HCO + CH_4 \quad (38)$$

$$CH_3 + CH_3 = C_2H_6 \quad (24)$$

$$C_2H_5 = C_2H_4 + H \quad (-15)$$

A substantial fraction of formaldehyde, methane, ethane, and ethylene diffuse upstream of this position, accounting for the significant concentrations of these species close to the burner surface.

At 1.4 mm above the burner surface, at a temperature of 1260 K, the concentration of DME is only 16% of that entering the flame. The fuel diffuses into this zone from a point upstream and is mainly consumed via hydrogen-atom abstraction by a hydroxyl radical and by hydrogen and oxygen atoms in a ratio of about 2.5:1.5:1. The resultant methoxymethyl radical decomposes to form formaldehyde and a methyl radical. Formaldehyde undergoes hydrogen-atom abstraction by H atoms and OH radicals at about the same rate, with the resultant formyl radical reacting with molecular oxygen and reacting by decomposition.

$$HCO + O_2 = CO + HO_2 \quad (46)$$

$$HCO = H + CO \quad (12)$$

$$HO_2 + H = OH + OH \quad (47)$$

Methyl radicals recombine to form ethane or react with hydroperoxy radicals to generate methoxy and hydroxyl radicals. Hydroperoxy radicals also react with hydrogen atoms to generate two hydroxyl radicals, as depicted above (R47). Hydroxyl radicals are also formed by the reaction of hydrogen atoms with molecular oxygen (R8) and by hydrogen-atom abstraction from the fuel by oxygen atoms.

Ethane undergoes hydrogen-atom abstraction by hydroxyl radicals and hydrogen atoms to generate ethyl radicals, which decompose to produce ethylene and a hydrogen atom.

$$C_2H_6 + OH = C_2H_5 + H_2O \quad (20)$$

$$C_2H_6 + H = C_2H_5 + H_2 \quad (17)$$

$$C_2H_5 = C_2H_4 + H \quad (-15)$$

The HCT edits indicate that substantial fractions of formaldehyde, methane, and ethane diffuse downstream of this position away from the burner surface. Ethylene undergoes hydrogen-atom abstraction mainly by OH and H to form vinyl radical. The vinyl radical then reacts with molecular oxygen to produce acetylene and hydroperoxy radical.

$$C_2H_4 + OH = C_2H_3 + H_2O \quad (62)$$

$$C_2H_4 + H = C_2H_3 + H_2 \quad (61)$$

$$C_2H_3 + O_2 = CH_2O + HCO \quad (112)$$

$$C_2H_3 + O_2 = C_2H_2 + HO_2 \quad (63, 85)$$

Carbon monoxide is generated by the reaction of formyl radicals with molecular oxygen (R46) and by the decomposition of formyl radicals (R12) in a ratio of about 2:1. In the rich DME flame discussed later, these reactions occur in the ratio 1:1, because of the lower concentration of molecular oxygen. Carbon monoxide and carbon dioxide mainly diffuse back into this zone from a point downstream, with convection carrying them downstream in a ratio of diffusion to convection of 2.5:1 and 4.4:1, respectively.

At 1.5 mm above the burner surface, at a temperature of 1320 K, the simulated concentration of DME is only 4% of that entering the flame. The underlying trends in this zone are similar to those observed at 1.4 mm. The fuel diffuses into this zone from a point upstream and is mainly consumed via hydrogen-atom abstraction by a hydroxyl radical and by oxygen and hydrogen atoms in a ratio of about 3:2:1. The concentration of formaldehyde is about 50% lower than its peak concentration because of its lower rate of production from the methoxymethyl radical and its higher rate of hydrogen-atom abstraction by hydroxyl radicals and hydrogen atoms, generating formyl radicals. The concentration of methane is only 25% lower than its peak value, as it is mainly generated by the reaction of methyl radicals with formyl radicals, H atoms, and hydroperoxy radicals.

$$CH_3 + HCO = CH_4 + CO \quad (39)$$

$$CH_3 + H = CH_4 \quad (1)$$

$$CH_3 + HO_2 = CH_4 + O_2 \quad (45)$$

The concentration of ethane is 50% below its peak value because of its oxidation to ethyl radicals via hydrogen-atom abstraction by OH, H, and O radicals. Ethylene is produced from the decomposition of ethyl radicals, and its concentration is about 90% of its peak value. It is consumed by reaction with hydroxyl radicals to form vinyl radical and water. The vinyl radical reacts with molecular oxygen to form formaldehyde or

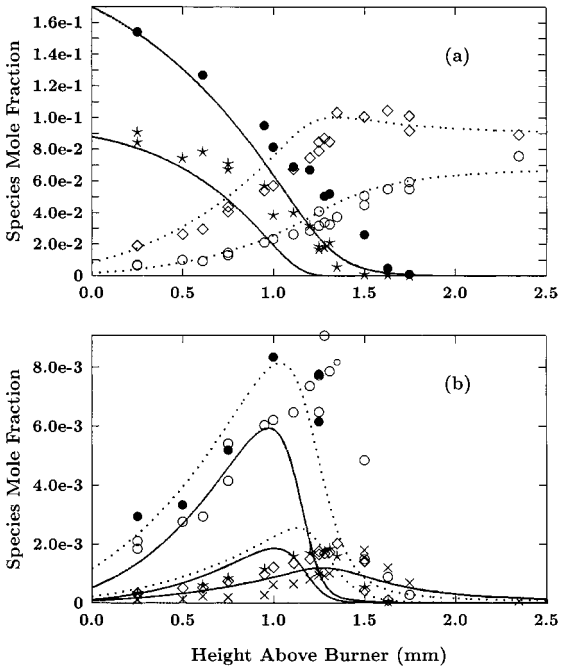

Figure 9. (a) Species mole fractions for the fuel-rich ($\phi = 1.49$) DME−air flame plotted as a function of sample probe position. ●, O_2; ○, CO_2; ★, CH_3OCH_3 ; and ◇, CO. (b) Symbols for the experimental data and computed peak concentrations for intermediate species (to aid curve identification) are ●, CH_2O (5900 ppm); ○, CH_4 (8080 ppm); ★, C_2H_6 (1820 ppm); ◇, C_2H_4 (2520 ppm); and ×, C_2H_2 (1180 ppm). Solid lines correspond to calculated mole fractions for filled and dotted lines to open symbols.

acetylene. Acetylene reaches its peak value (50 ppm) in this zone. It is consumed by reaction with atomic oxygen and is also lost via diffusion downstream.

$$C_2H_2 + O = HCCO + H \quad (87)$$

$$C_2H_2 + O = CH_2 + CO \quad (69)$$

Carbon monoxide also reaches its peak at 1.5 mm. It is mainly produced by the reaction of formyl radicals with molecular oxygen and by formyl-radical scission in a ratio of 1:1. Carbon monoxide is controlled by diffusion toward the burner surface and by reaction with hydroxyl radicals to generate carbon dioxide and hydrogen atom.

Finally, at a distance of 1.7 mm above the burner surface, at a temperature of 1445 K, most of the computed fuel and intermediate species have been converted to carbon dioxide.

Rich Dimethyl Ether Flame. Modeling simulations of the rich ($\phi = 1.49$) DME flame show that both the widths and peak heights of the reactant, intermediate, and product species profiles compare well with the experimental results (Figure 9). However, there is an apparent shift of about 0.2 mm toward the burner surface in the species concentration profiles, which may be due to the uncertainty in position of the measured temperature profile used in the simulation.

The peak concentrations of methane and formaldehyde occur at a distance of between 0.9 and 1.0 mm above the burner surface indicating that this is the position at which chemistry is controlling the oxidation of the fuel and intermediate products. As for the lean DME flame, analysis of HCT edits indicates that diffusion and convection downstream are the main factors controlling fuel and oxygen consumption up to 0.9 mm, where the temperature is 1180 K. Here, the fuel undergoes hydrogen-atom abstraction by hydrogen atoms and by hydroxyl and methyl radicals in the ratio 6.6:2.7:1. This ratio is 3:5:1 in the fuel-lean DME flame, thus indicating the more dominant role played by hydrogen atoms in the rich flame. In addition, a comparison of the chemistry controlling formaldehyde oxidation in the rich flame indicates that abstraction by hydroxyl radicals has about one-third the importance observed in the lean flame. Overall, there are lower concentrations of hydroxyl radicals in the rich flame relative to those in the lean flame. Hydroxyl radicals are generated from hydroperoxy radicals either by their reaction with a methyl radical (which generates one hydroxyl radical) or a hydrogen atom (which generates *two* hydroxyl radicals), whereas hydroperoxy radicals are produced by the reaction of formyl radicals with molecular oxygen.

$$HO_2 + CH_3 = CH_3O + OH \quad (22)$$

$$HO_2 + H = OH + OH \quad (47)$$

$$HCO + O_2 = CO + HO_2 \quad (46)$$

The lower relative concentration of molecular oxygen in the rich flame results in a lower overall rate of production of hydroperoxy radicals, and consequently, the concentration of hydroxyl radicals is lower in the rich flame relative to the lean flame. In addition, the lower concentration of molecular oxygen also results in a lower relative rate of its reaction with hydrogen atoms in the chain branching reaction, which also produces hydroxyl radicals.

$$H+O_2 = O + OH \quad (8)$$

With respect to intermediate species profiles in both the rich and lean DME flames (Figures 8b and 9b), high concentrations of formaldehyde are measured and predicted in both flames. However, much higher concentrations of methane, ethane, and ethylene are observed in the rich flame relative to the lean flame. In the lean flame, the predicted peak concentrations are 1440, 949, and 576 ppm, respectively, whereas in the rich flame they are 2−10 times higher, being 8140, 1860, and 2550 ppm, respectively. The higher concentrations of these hydrocarbons result from the lower concentration of hydroperoxy radicals present in the rich flame relative to the lean flame. This reduces the rate of consumption of methyl radicals by hydroperoxy radicals in the rich flame, increasing the CH_3 mole fraction. Consequently, in the rich flame, both the rate of methyl-radical recombination to generate ethane, which subsequently forms ethylene and acetylene, and the rate of methyl radicals abstracting a hydrogen atom from the fuel to generate a methoxymethyl radical and methane, are enhanced relative to the lean flame. The ratio of carbon monoxide to carbon dioxide is greater in the rich flame relative to the lean flame because of the effect of equivalence ratio on the thermodynamic equilibrium.

Methane Flames. Figures 10 and 11 depict species concentration profiles versus height above the burner surface for the lean ($\phi = 0.74$) and rich ($\phi = 1.47$) methane flames. The main species measured experimentally were methane and molecular oxygen, together with the main oxidation products CO, CO_2, CH_2O, C_2H_6, C_2H_4, and C_2H_2. In the lean methane flame, the measured concentration of formaldehyde is approximately 4 times lower than that measured in the lean DME flame. In the rich methane flame, CH_2O is approximately an order of magnitude lower than that measured in the rich DME flame.

For all species except C_2H_2 in the rich flame, the model-predicted concentration profiles for the methane flames are in good agreement with the experimental measurements. In the

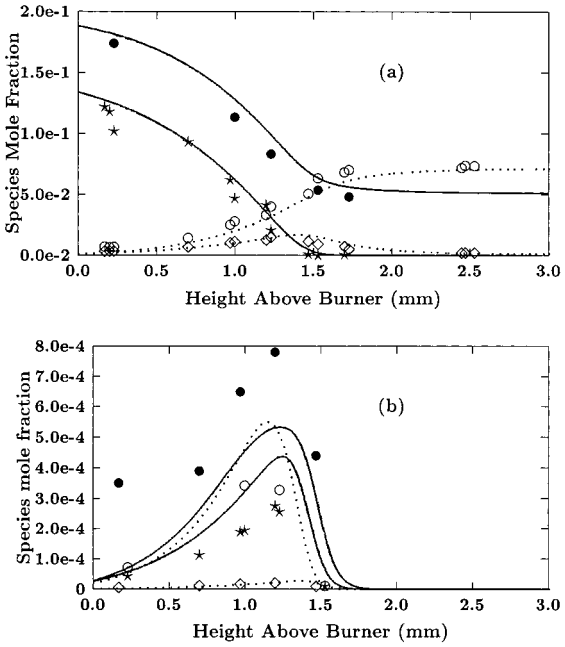

Figure 10. (a) Species mole fractions for the fuel-lean ($\phi = 0.74$) methane−air flame plotted as a function of sample probe position. ●, O_2; ○, CO_2; ★, CH_4; and ◇, CO. Experimental O_2 profile has been adjusted by 0.8 in order to account for miscalibration (see Experimental Measurements section). (b) Symbols for the experimental data and computed peak concentrations for intermediate species (to aid curve identification) are ●, CH_2O (530 ppm); ○, C_2H_6 (550 ppm); ★, C_2H_4 (430 ppm); and ◇, C_2H_2 (30 ppm). Solid lines correspond to calculated mole fractions for filled and dotted lines to open symbols.

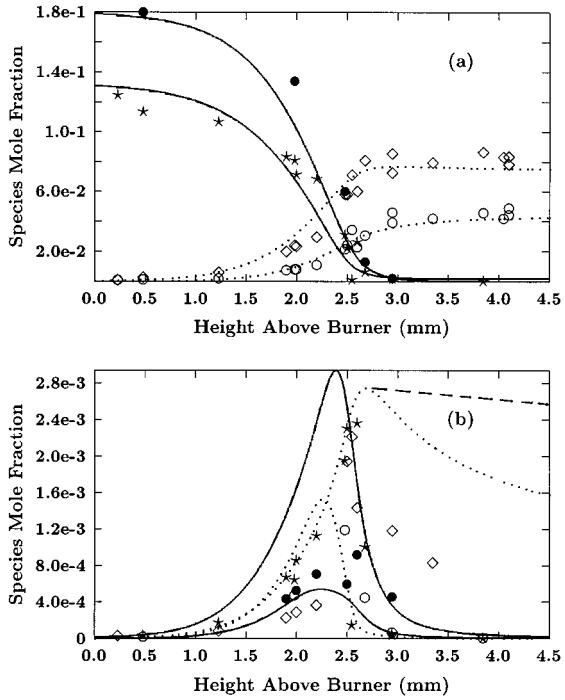

Figure 11. (a) Species mole fractions for the fuel-rich ($\phi = 1.47$) methane−air flame plotted as a function of sample probe position. ●, O_2; ○, CO_2; ★, CH_4; and ◇, CO. (b) Symbols for the experimental data and computed peak concentrations for intermediate species (to aid curve identification) are ●, CH_2O (530 ppm); ○, C_2H_6 (1530 ppm); ★, C_2H_4 (2960 ppm); and ◇, C_2H_2 (2760 ppm). Solid lines correspond to calculated mole fractions for filled and dotted lines to open symbols. The dashed line in panel b is the computed C_2H_2 profile in the post-flame gas using the Miller−Melius acetylene mechanism (see text).

post-flame gas of the rich flame, the experimental measurements show that the concentration of acetylene decreases by a factor of approximately 3 between 2.5 and 3.5 mm above the burner surface. The model, which originally contained the acetylene submechanism derived from Miller and Melius,[23] predicted that very little acetylene consumption occurs in the post-flame gas up to a height of 4.5 mm (see dashed line in Figure 11b). To obtain the simulated profile (dotted line) shown in Figure 11b, which still underpredicts the acetylene consumption, we have adopted the rate expression of 3.24×10^{13} exp(−12 000 cal/*RT*) cm^3 mol^{-1} s^{-1} recommended by Kaiser[24] for the reaction $C_2H_2 + OH = CH_2CO + H$. Previously, Kaiser found it necessary to use this rate expression, which is approximately 10 times faster than that recommended by Miller and Melius at 1800 K, to accurately predict the acetylene profile measured in a propane−air flame. It is clear that further validation of the current acetylene submechanism is needed.

In the lean methane flame, the model indicates that the fuel and molecular oxygen diffuse and convect downstream, away from the burner surface, as in the DME flames and the rich methane discussed later. Most of the chemistry occurs at 1.1−1.3 mm above the burner surface. In this region, the main reactions consuming methane are hydrogen-atom abstraction by OH radicals and by H and O atoms, in a ratio of about 4:2:1.

$$CH_4 + OH = CH_3 + H_2O \quad (3)$$

$$CH_4 + H = CH_3 + H_2 \quad (2)$$

$$CH_4 + O = CH_3 + OH \quad (4)$$

At 1.1 mm above the burner, where the temperature is 1110 K, methyl radicals recombine to form ethane, react with hydroperoxy radicals to generate methoxy and hydroxyl radicals, and react with atomic oxygen to generate formaldehyde and hydrogen atom in the ratio 8:2:1.

$$CH_3 + CH_3 = C_2H_6 \quad (24)$$

$$CH_3 + HO_2 = CH_3O + OH \quad (22)$$

$$CH_3 + O = CH_2O + H \quad (36)$$

At 1.3 mm above the burner surface, where the temperature is 1290 K, the increase in the rate of the chain branching $H + O_2 = O + OH$ reaction results in higher concentrations of oxygen atoms, and thus, the ratio of the three reactions above becomes 5:1:4. The methoxy radical decomposes to form a hydrogen atom and formaldehyde.

The chemistry associated with formaldehyde, ethane, ethylene and acetylene is very similar to that observed in the lean DME flame. At 1.4 mm, formaldehyde undergoes hydrogen-atom abstraction by OH radicals and by H and O atoms to generate formyl radicals, which scission to form carbon monoxide and hydrogen atoms (R12) and react with molecular oxygen to produce carbon monoxide and a hydroperoxyl radical (R46) in the ratio of about 1:1. Ethane undergoes hydrogen-atom abstraction by hydroxyl radicals and by oxygen and hydrogen atoms to generate ethyl radicals, which decompose to form ethylene and a hydrogen atom and react with molecular oxygen to generate ethylene and a hydroperoxyl radical in the ratio 1:1. Ethylene reacts with atomic oxygen to form methyl and formyl radicals and also reacts with hydroxyl radicals to generate a vinyl radical and water. The vinyl radical then reacts with molecular oxygen to generate acetylene and hydroperoxyl radical.

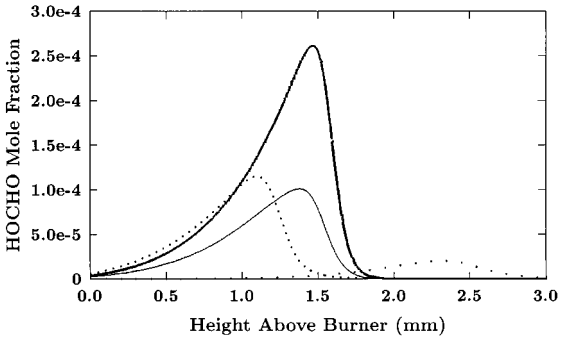

Figure 12. Comparison of model-predicted formic acid concentrations for each flame plotted as a function of sample probe position: lean CH_3OCH_3 (bold solid line); rich CH_3OCH_3 (close-spaced dotted line); lean CH_4 (solid line); rich CH_4 (far-spaced dotted line).

In the rich methane flame, most of the chemistry occurs at 2.1−2.4 mm above the burner surface, where the temperature is in the range 1070−1470 K. In this region, the main reactions consuming methane are hydrogen-atom abstraction by H atom and OH radical, in a ratio of about 2:1. As in the DME flames, the importance of hydroxyl radicals is lower in the rich flame relative to the lean flame because of the lower relative concentration of molecular oxygen.

In all four flames, the main chemistry occurs in the temperature range 1100−1200 K. This phenomenon is due to the chain branching reaction

$$H + O_2 = O + OH \tag{8}$$

which generates two reactive radicals from one reactive hydrogen atom and a stable molecule.

One final point of interest is that the model predicts formic acid to be formed in concentrations above the experimental detection limit (100 ppm) of our system in the lean DME flame. Formic acid is predicted to be formed via the addition of hydroxyl radical to formaldehyde and subsequent decomposition of the intermediate HOCH2O radical species to formic acid and a hydrogen atom.

$$CH_2O + OH = HOCH_2O^* = HOCHO + H$$

Figure 12 shows the concentrations of formic acid predicted in each flame. In particular, the lean DME flame predicts concentration of formic acid almost three times higher than the detectable limit. The concentrations predicted for the rich DME and lean methane flames just reach detectable levels, whereas that for the rich methane flame is below the detectable limit. However, it is not surprising that the predicted concentration of formic acid is largest in the lean DME flame as the concentrations of formaldehyde and hydroxyl radical are also highest in this flame. Niki et al.[25] studied the reaction of hydroxyl radicals with formaldehyde at a temperature of 299 K and a pressure of 700 Torr and found that formaldehyde exclusively undergoes abstraction rather than addition. However, Stief et al.[26] have proposed that pressure dependence in k(OH + CH_2O) may be expected, as the addition reaction is likely to proceed via a chemically activated adduct. This issue is also discussed in our modeling of a separate work on the low-temperature oxidation of dimethyl ether in a flow reactor.[9] We have employed a high-pressure-limit expression for the addition of hydroxyl radical to formaldehyde, and therefore, at 1 atm pressure we expect to overestimate the concentration of formic acid produced.

Conclusions

Experimental profiles for reactant, stable intermediate, and final product species have been measured in premixed, atmospheric-pressure, fuel−air flat flames as a function of sample probe height above a flat-flame burner. The two fuels studied were dimethyl ether (the primary focus of this study) and methane (as a reference flame). Species profiles for each fuel were measured at a fuel-lean ($\phi \approx 0.7$) and a fuel-rich ($\phi \approx 1.5$) equivalence ratio at similar cold-gas flow velocities. Temperature profiles throughout the flame were determined for each flame condition using the sample probe as a pneumatic temperature-measuring device that was calibrated in the burned gas by a thin-wire thermocouple. The experimental results showed that the peak mole fractions of the intermediate organic species (with the exception of CH_2O) in the DME flame were similar to those in the methane flame at both equivalence ratios. The CH_2O mole fractions in the DME flames were 4 ($\phi = 0.67$) and 10 ($\phi = 1.49$) times larger than their methane-flame counterparts. These results suggest that decomposition of the CH_3OCH_2 radical (e.g., $CH_3OCH_2 = CH_3 + CH_2O$), which is formed by the initial free radical attack on DME, plays a crucial role in the structure of the DME flame. This decomposition reaction yields formaldehyde and a methyl radical, consistent with the observation that C_2 hydrocarbons are formed in similar mole fraction to those in the CH_4 flames, which also generate methyl radicals in their initial reaction step. The increased formaldehyde in the DME flames can also be rationalized on the basis of this reaction, which does not occur in methane flames.

A computational study of these four flames was carried out using two burner-stabilized flame codes, HCT and Chemkin III. Initially, comparisons of the predicted major species profiles for one methane and one DME flame were carried out using both codes. The predicted species profiles for the two flame codes agreed satisfactorily, albeit not exactly. The computed peak mole fractions of reactant, intermediate, and product species agreed to within 30% with the experimental peak mole fractions for all flames except the lean DME flame. For this flame, the intermediate hydrocarbon species mole fractions, with the exception of CH_2O, were over predicted by factors of approximately 3. The latter flame was observed experimentally to have an unusually thick luminous zone and broader intermediate species profiles than the other flames. This difference was not captured by the model, which predicted narrower species profiles and a faster consumption of DME in this flame, probably leading to the overprediction of the peak intermediate species mole fractions relative to experiment. However, it is important to note that overall the predicted species profiles show satisfactory agreement with the measured species profiles, both in shape and peak mole fraction. This indicates that the basic mechanism used in this study provides an essentially correct representation of DME oxidation in a flame.

The modeling study verifies the importance of the decomposition of the methoxymethyl radical described above. This reaction is the major source of formaldehyde in the DME flames and provides the methyl radical needed to form the observed C_2 species. The agreement between experiment and simulation for peak species mole fractions and profile shapes in both methane flames verifies that, when a well-established chemical kinetic mechanism is available, agreement between experiment and model is satisfactory. However, the discrepancy between the experiment and the model in the lean DME flame indicates that the mechanism used in this computational model may need improvement, perhaps related to the possible existence of reactions

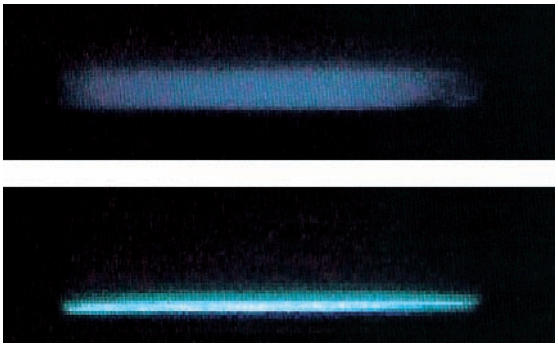

Figure A-1. Edge-on photograph (*f*3.4, 1/60 s) of flat-flame burner fueled by DME: top ($\phi = 0.67$); bottom ($\phi = 1.49$). Diameter of flame disk = 6.0 cm. Scale of vertical axis has been expanded by a factor of 4 relative to the horizontal axis for clarity.

of activated $CH_3OCH_2O_2$ radicals, which have been inferred on the basis of room-temperature experiments of DME oxidation.

Photographic observations of DME, methane, and ethane diffusion flames stabilized on a Meeker burner, as presented in the Appendix, have demonstrated that the luminosity of the DME flame is much less intense than that of an ethane flame having the same volume (and, therefore, carbon + hydrogen mass) flow rate. This result suggests that soot generation in a DME diffusion flame (which is present in a diesel engine combustion chamber) is inherently less than that generated by longer-chain hydrocarbon fuels, an observation consistent with the low exhaust particulate emission from a diesel-powered, DME-fueled vehicle. DME does produce soot emission when the rate of fuel flow is increased by 50%, as might be expected on the basis of the observed formation of higher-molecular-weight (C_2 and C_3) hydrocarbon species in the flame zone of the flat-flame burner, but the luminosity is still much lower than that of the ethane flame.

Acknowledgment. The computational portions of this work were supported by the U.S. Department of Energy, Office of Transportation Technologies, and performed under the auspices of the U.S. Department of Energy by the Lawrence Livermore National Laboratory under Contract W-7405-ENG-48.

Appendix

Flame Thickness. Figure A-1 presents edge-on, digital photographs of the lean and rich DME flat flame using identical aperture and exposure time (*f*3.4, 1/60 s). The scale of the photograph can be determined by noting that the diameter of the flame disk is 6.0 cm and that the scale of the vertical axis has been expanded by a factor of 4 relative to the horizontal dimension to provide better clarity in measuring the flame thickness. The thickness of the lean flame is 1.5 mm, whereas that of the rich flame is 0.4 mm for the very bright band and 0.65 mm including the much dimmer region.

Particulate Emissions. A major reason for this study of the combustion chemistry of DME is to shed more light on the particulate formation process in DME flames. As mentioned in the Introduction, DME is a good diesel engine fuel that produces very low particulate emissions in contrast to conventional fuels. Two possibilities could explain the lack of particulate emissions. First, the chemistry of DME might be such that little particulate matter is formed during its combustion. This is the case for methanol flames because the initial step in methanol combustion leads to the production of either CH_3O or CH_2OH radicals, which are rapidly converted to CH_2O and thence to CO and CO_2. Thus, in moderately rich methanol flames, no particulates

Figure A-2. Photograph (*f*2.4, 1/60 s) of DME Meeker burner diffusion flame. DME volume flow = 330 $cm^3\ min^{-1}$.

are generated because essentially no CH_3 radicals are formed, and these radicals are the source of the higher-molecular-weight hydrocarbons which can lead to soot generation. This is the reason pool fires of methanol are very dangerous because they produce no particulates, and, therefore, essentially no luminosity that can warn of the presence of fire. The second possibility is that DME does not form appreciable particulate emissions simply because DME is a gaseous rather than a liquid fuel. The absence of liquid droplets in the engine cylinder during fuel injection can markedly reduce soot generation by incomplete combustion of these liquid droplets and can promote more complete mixing of the fuel with air during the fuel injection process.

To explore this question, atmospheric-pressure diffusion flames of three gaseous fuels (CH_4, C_2H_6, and DME) were photographed by a digital camera using identical apertures and exposure times (*f*2.4, 1/60 s). These flames were stabilized on a Meeker burner, 3.5 cm in diameter, whose air intake slots had been sealed to preclude introduction of air into the fuel exiting the top of the burner, thus providing a pure diffusion flame. In these experiments, the mass flow rate of carbon + hydrogen was maintained essentially constant for all three fuels. This was done because CH_n combustion provides the source of heat release in all of these fuels, and in a diesel engine, the amount of heat released will be similar for all fuels under similar operating conditions. Therefore, the volume flow rates of ethane and DME were adjusted to be nearly identical (220 and 215 $cm^3\ min^{-1}$, respectively), while the volume flow rate of methane was twice as large (440 $cm^3\ min^{-1}$), because it has only one carbon atom. Pictures of each of these flames are shown in Figure A-3. The luminosities are very different from one another, and luminosity is a measure of the particulate loading within the flame. Very little luminosity is observed from the DME diffusion flame, whereas that of the ethane flame is very bright. Methane produces a luminous flame but one that is much less bright than that of ethane. The ethane flame produces sufficient luminosity to cause reflections from the Pyrex chimney that shields the burner from air currents, as shown in the figure. These photographs indicate that, at this mass flow condition, DME generates much less particulate mass than does ethane. When the volume flow of DME is increased to 335 $cm^3\ min^{-1}$, the DME flame produces visible luminosity (Figure A-2) comparable to that of methane fuel at the lower carbon mass

Figure A-3. Photographs (*f*2.4, 1/60 s) of Meeker burner diffusion flames: top = ethane (220 cm^3 min^{-1}); middle = methane (440 cm^3 min^{-1}); bottom = DME (215 cm^3 min^{-1}).

flow rate. Thus, under the appropriate conditions, DME does produce soot, as might be expected from the observation in the flat-flame-burner experiments that C_2 species are produced in the DME flame front. However, the fact that DME produces much less luminosity than an ethane flame at the same volume (and carbon mass) flow rate, indicates that the low soot emission from DME in a diesel engine may result from the fact that combustion of DME in a diffusion flame inherently produces lower soot formation rates at the same operating condition than do most hydrocarbon fuels. This may result partially from the fact that DME carries some oxygen in its molecular structure, which may reduce particulate formation in a diffusion flame. The fact that it is a gas probably also lowers the soot emission even further relative to that of a liquid fuel in diesel-fueled vehicles.

References and Notes

(1) Fleisch, T.; McCarthy, C.; Basu, A.; Udovich, C.; Charbonneau, P.; Slodowske, W.; Mikkelsen, S.-E.; McCandless, J. *SAE Tech. Pap. Ser.* **1995**, 950061.

(2) Sorenson, S. C.; Mikkelsen, S.-E. *SAE Tech. Pap. Ser*. **1995**, 950064.

(3) Kapus, P. E.; Cartellieri, W. P. *SAE Tech. Pap. Ser*. **1995**, 952754.

(4) Kajitani, S.; Chen, Z. L.; Konno, M.; Rhee, K. T. *SAE Tech. Pap. Ser*. **1997**, 972973.

(5) Verbeek, R.; Van der Weide, J. *SAE Tech. Pap. Ser*. **1997**, 971607.

(6) Fleisch, T. H.; Basu, A.; Gradassi, M. J.; Masin, J. G. Dimethyl ether: a fuel for the 21st century. In *Natural Gas Conversion IV*; de Pontes, M., Espinoza, R. L., Nicolaides, C. P., Scholtz, J. H., Scurrell, M. S., Eds.; Studies in Surface Science and Catalysis, Elsevier Science B. V.: New York, 1997; Vol. 107.

(7) Rouhi, A. M. *Chem. and Eng. News* **1995**, May 29, 37.

(8) Curran, H. J.; Pitz, W. J.; Westbrook, C. K.; Dagaut, P.; Boettner, J.-C.; Cathonnet, M. *Int. J. Chem. Kinet*. **1998**, *30*, 229.

(9) Curran, H. J.; Fischer, S. L.; Dryer, F. L. *Int. J. Chem. Kinet*., in press.

(10) Fischer, S. L.; Dryer, F. L. Curran, H. J. *Int. J. Chem. Kinet*., in press.

(11) Kaiser, E. W.; Rothschild, W. G.; Lavoie, G. A. *Combust. Sci. Technol*. **1984**, *41*, 271.

(12) Kaiser, E. W.; Marko, K.; Klick, D.; Rimai, L.; Wang, C. C.; Shirinzadeh, B., Zhou, D. *Combust. Sci. Technol*. **1986**, *50*, 163.

(13) Taylor, C. F. *The Internal Combustion Engine in Theory and Practice*, 2nd ed.; The MIT Press: Cambridge, MA, 1966; Vol. 1, pp 503−507 (see eq A-14, modified for choked flow).

(14) Fristrom, R. M. *Flame Structure and Processes*; Oxford University Press: New York, 1995; p 124.

(15) Rothschild, W. G.; Kaiser, E. W.; Lavoie, G. A. *Combust. Sci. Technol*. **1986**, *47*, 209.

(16) Kee, R. J.; Warnatz, J.; Miller, J. A. *A Fortran Computer Code Package for the Evaluation of Gas-Phase Viscosities, Conductivities and Diffusion Coefficients*; SAND83-8209; Sandia National Laboratories: Livermore, CA, 1983.

(17) Marinov, N. M.; Pitz, W. J.; Westbrook, C. K.; Lutz, A. E.; Vincitore, A. M.; Senkan, S. M. *Twenty-Seventh Symposium (International) on Combustion*; The Combustion Institute: Pittsburgh, PA, 1998; pp 605−613.

(18) Reid, C.; Prausnitz, J. M.; Poling, B. E. In *The Properties of Gases and Liquids*, 4th ed.; McGraw-Hill: New York, 1987.

(19) Kee, R. J.; Rupley, F. M.; Meeks, L. M.; Miller, J. A. *A Fortran Chemical Kinetics Package for the Analysis of Gas-Phase Chemical Kinetics*; SAND96-8216; Sandia National Laboratories: Livermore, CA, 1996. *CHEMKIN Collection III*, Reaction Design, Inc.: San Diego, CA, 1999.

(20) Kee, R. J.; Grcar, J. F.; Smooke, M. D.; Miller, J. A. *A Fortran Program for Modeling Steady Laminar One-Dimensional Premixed Flames*; SAND85-8240; Sandia National Laboratories, Livermore, CA, 1985. *CHEMKIN Collection III*, Reaction Design, Inc.: San Diego, CA, 1999.

(21) Lund, C. M.; Chase, L. HCT−*A General Computer Program for Calculating Time-Dependent Phenomena Involving One-Dimensional Hydrodynamics, Transport, and Detailed Chemical Kinetics*; Report UCRL-52504; Lawrence Livermore National Laboratory: Livermore, CA, revised 1995.

(22) Sehested, J.; Mogelberg, T.; Wallington, T. J.; Kaiser, E. W.; Nielsen, O. J. *J. Phys. Chem.* **1996**, *100*, 17218.

(23) Miller, J. A.; Melius, C. F. *Combust. Flame* **1992**, *91*, 21.

(24) Kaiser, E. W. *J. Phys. Chem.* **1990**, *94*, 4493.

(25) Niki, H.; Maker, P. D.; Savage, C. M.; Breitenbach, L. P. *J. Phys. Chem.* **1984**, *88*, 5342.

(26) Stief, L. J.; Nava, D. F.; Payne, W. A.; Michael, J. V. *J. Chem. Phys.* **1980**, *73*, 2254.